Composites Communications 25 (2021) 100696

Contents lists available at ScienceDirect

Composites Communications

journal homepage: www.elsevier.com/locate/coco

Radical-functionalized polymer nanofiber composite separator for ultra-stable dendritic-free lithium metal batteries

Chunyang Zhou, Wei Zong, Gangyong Zhou, Xiaoshan Fan, Yue-E Miao *

State Key Laboratory for Modification of Chemical Fibers and Polymer Materials, College of Materials Science and Engineering, Innovation Center for Textile Science and Technology, Donghua University, Shanghai, 201620, PR China

ARTICLE INFO

Keywords:
Radical-functionalization
Electrospinning
Composite separator
Lithium metal battery

ABSTRACT

The application of lithium-metal batteries (LMBs) is limited to the high reactivity of lithium with electrolytes and uncontrolled dendritic Li formation. Therefore, to achieve the uniform deposition of Li from metal crystallization nucleation stage is of great significance for the realization of dendritic-free Li anode. Herein, a polymethyl methacrylate (PMMA) precursor grafted with 9-anthracenecarboxylic acid (An) and 4-amino-2,2,6,6-tetramethyl-1-piperidinylox (TEMPO) has been directly electrospun on the surface of the commercial polypropylene (PP) separator to obtain a radical functionalized bilayer porous composite membrane, which is signed as PMMA-An/TEMPO@PP. The radical functional groups of TEMPO can guide the uniform distribution of Li nucleation while the cross-linked An groups can improve the mechanical strength of the composite nanofiber membrane. Furthermore, the three-dimensionally interconnected porous nanofiber network can evenly redistribute the lithium ions when they pass through the composite separator. As a result, at a high current density of 2 mA cm^{-2}, the lithium metal anode achieves a high Coulomb efficiency (97%) for uniform and dendrite-free deposition of lithium, as well as a long-term reversible lithium plating/stripping of 950 h for potential applications in LMBs.

1. Introduction

With the rapid development of portable devices and electric vehicles, there is a growing demand for energy storage devices with high energy density and long cycle life [1–6]. Currently, rechargeable lithium-ion batteries (LIBs) have been extensively applied in commercial applications. However, owing to the theoretical specific capacity limitations of the carbonaceous anodes and metal oxide-based cathodes, traditional LIBs can hardly meet the increasing demands for emerging energy devices [7–13]. As a promising alternative candidate beyond LIBs, lithium metal batteries (LMBs) based on metallic Li have attracted much attention for the highest theoretical capacity (3860 mAh g^{-1}) and lowest electrochemical potential (−3.04 V vs the standard hydrogen electrode) of Li [14–18]. However, the commercialization application of lithium metal anodes in LMBs remains difficult, which are mainly due to the highly reactive nature of Li and uncontrolled dendritic Li formation [19–21].

On the one hand, caused by the inevitable microscopic roughness of the electrode surface, the nearby electric field is not evenly distributed during charging/discharging process, which would lead to the preferential deposition of lithium metal at the tip of the bulges [22–25]. During battery operation, this phenomenon will be severely intensified, thus resulting in the formation of Li dendrites. The continuing growth of Li dendrites further bridges the inter-electrode space and causes internal short circuits in the cells, which gives rise to obvious safety risks [26, 27]. On the other hand, the active Li metal irreversibly consumes the electrolyte to form a solid electrolyte interphase (SEI). But the non-uniform deposition causes significant volume change of Li metal during the plating/stripping process, which makes the fresh Li metal constantly exposed to the electrolyte. This will lead to the continuous consumption of Li metal and electrolyte in repeated plating/stripping process, which gradually reduces the Coulomb efficiency and results in poor cycling stability [28].

To stabilize the lithium metal anode, researchers have tried various methods, including developing structured Li metal anodes, artificial SEI, optimized electrolyte compositions, solid-state electrolytes, and modified current collectors [29–31]. Nevertheless, the high reactivity of lithium makes the structured Li metal anodes or current collectors very difficult for large-scale industrial operations. Besides, although the optimized electrolytes are intended to form a more stable SEI, the in-situ

* Corresponding author.
E-mail address: yuee_miao@dhu.edu.cn (Y.-E. Miao).

https://doi.org/10.1016/j.coco.2021.100696
Received 6 February 2021; Received in revised form 20 February 2021; Accepted 20 February 2021
Available online 4 March 2021

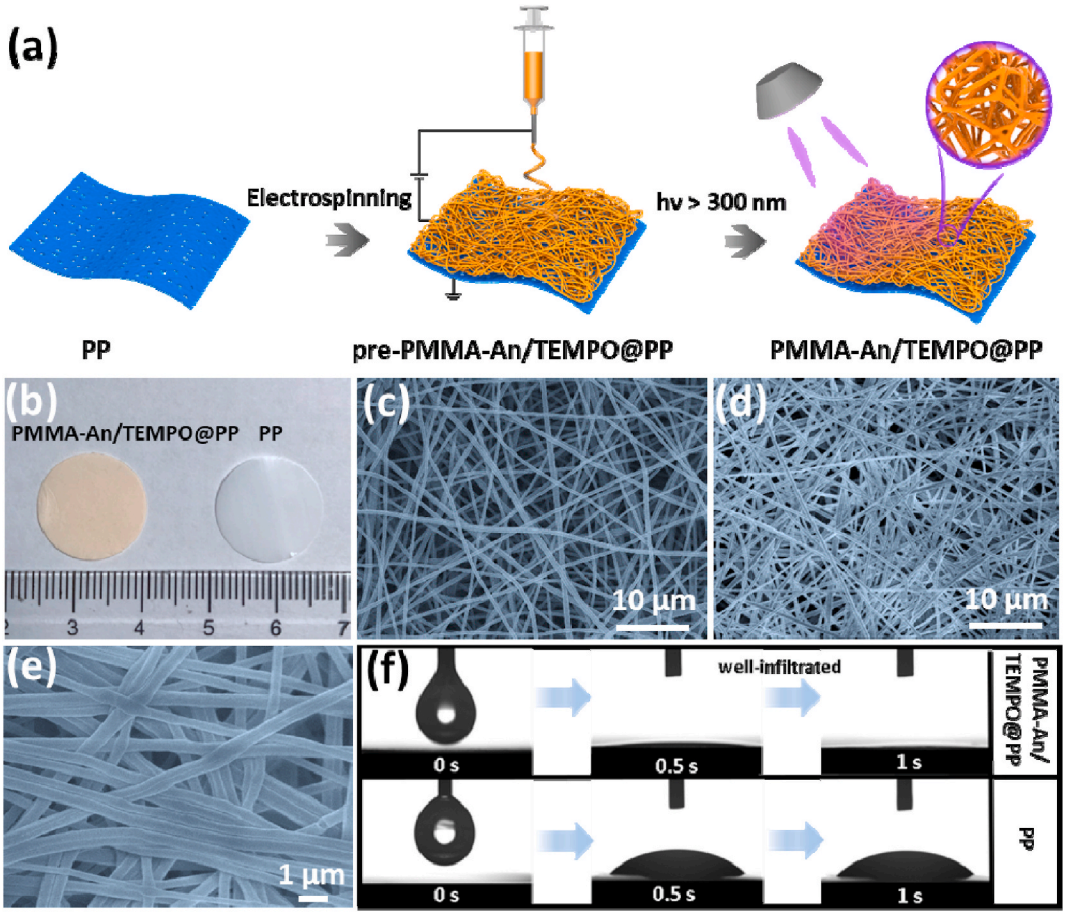

Fig. 1. (a) Schematic illustration of the synthesis process for the PMMA-An/TEMPO@PP separator. (b) Digital photographs of PMMA-An/TEMPO@PP and PP separators. SEM images of (c) pre-PMMA-An/TEMPO@PP and (d, e) PMMA-An/TEMPO@PP separators. (f) Contact angle of electrolyte on PP and PMMA-An/TEMPO@PP separators.

formed SEI layers can still hardly prevent the growth of lithium dendrites completely [32]. It is well known that as an indispensable component of batteries, the separator plays a crucial role in the electrochemical performance, which not only prevents short circuit by polar contact but also provides porous channels for lithium-ion migration. As a result, the performance of separators significantly affects the internal resistance and interfacial structure of the batteries. Nonetheless, few works have comprehensive reports about separators with abundant polar groups to deposit lithium metal uniformly [33]. Therefore, the development of high-performance separators to fundamentally inhibit the formation of Li dendrites and achieve stable Li deposition/exfoliation is of great significance to the stable operation of LMBs.

Recently, some modification strategies of polyolefin separators have been reported to achieve the purpose of uniform lithium-ion flux distribution, such as vacuum filtration technique, the slurry coating process, and magnetron sputtering [34]. However, these strategies generally incorporate complex operation processes, which are difficult to be costly controlled. Furthermore, it is still a critical issue to efficiently improve the interfacial interactions between the modification layers and polyolefin separators. Considering the simplicity and versatility of electrospinning technique for a wide variety of precursor materials [35], electrospun polymer nanofiber separators with unique features of easy functionalization, controllable nanofiber diameter and pore size show great potentials for LMB applications.

Herein, a radical functionalized bilayer porous composite membrane has been prepared by the direct electrospinning of polymethyl methacrylate (PMMA) grafted with 9-anthracenecarboxylic acid (An) and 4-amino-2,2,6,6-tetramethyl-1-piperidinylox (TEMPO) nanofiber layer on the surface of the commercial polypropylene (PP) separator, which is signed as PMMA-An/TEMPO@PP composite separator for LMB applications. It is exciting that a large number of polar groups including the C═O and nitroxyl radical groups of TEMPO are introduced within the uniquely interconnected PMMA nanofiber microchannels, which can provide high concentration of functional sites for the rapid distribution and uniform flux of Li ions. Thus, uniform deposition of Li ions and stable operation of Li metal anode can be achieved under high current densities. Besides, the An groups can improve the mechanical strength of the nanofiber membrane after crosslinking under ultraviolet light. As a result, the cell assembled by PMMA-An/TEMPO@PP composite separator exhibits dendritic-free homogeneous Li deposition with high Coulomb efficiency and ultralong-term reversible Li plating/stripping, which indicates potential prospect in guarantee the safety and long cycling stability of LMBs.

2. Experimental section

2.1. Materials

Polymethyl methacrylate (PMMA, M_w = 350000), 4-amino-2,2,6,6-tetramethyl-1-piperidinylox (TEMPO, AR), 9-Anthracenecarboxylic acid (An, AR), 4-Dimethylaminopyridine (DMAP) and 1-ethyl-3-(3-dimethyllaminopropyl) carbodiie hydrochlide (EDC.HCl) were purchased from TCI, Tokyo Chemical Industry Co., Ltd, Tokyo, Japan. 2-Aminoethanol (AH, 99%), *N,N*-dimethylformamide (DMF, 99.9%) and *N*-methyl pyrrolidone (NMP, 99%) were supplied by Sigma-Aldrich. Deionized (DI) water was used throughout the experiments. All

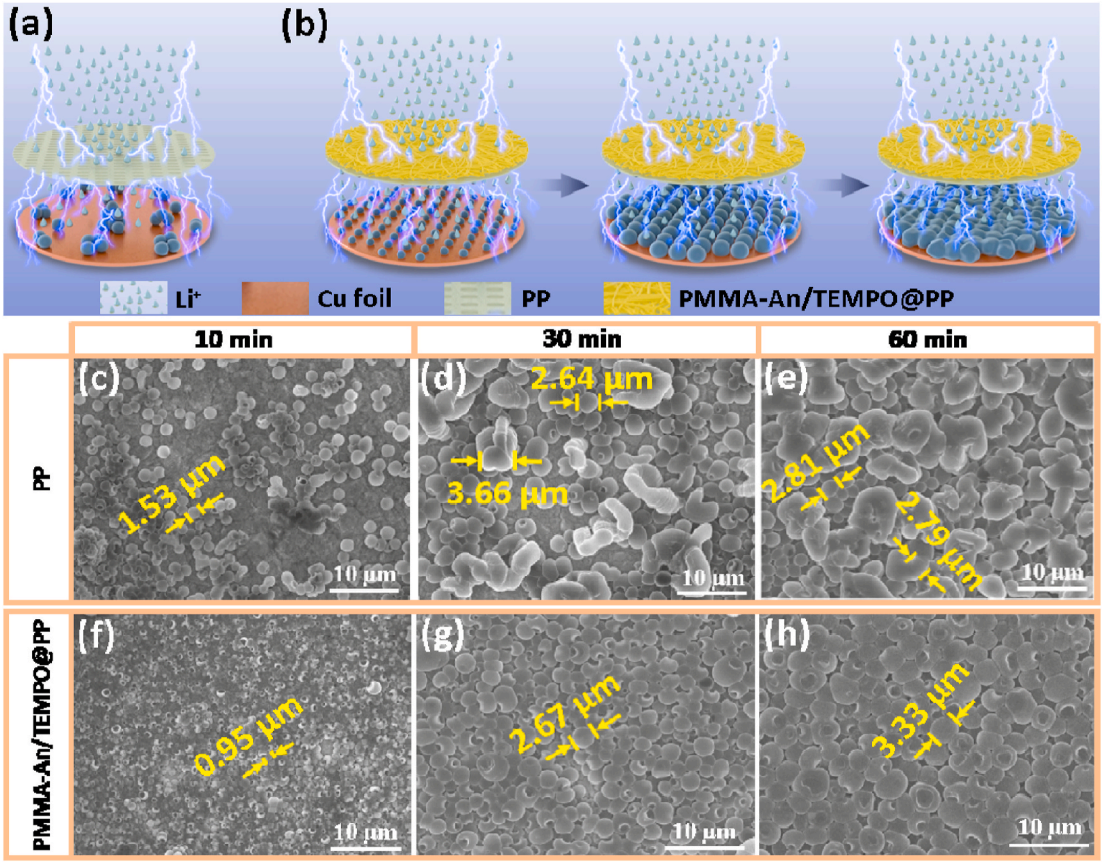

Fig. 2. Schematics showing Li deposition on the electrode with (a) PP and (b) PMMA-An/TEMPO@PP separators during charging/discharging. SEM images of Li deposition on the Cu foils at 1 mA cm^{-1} for 10 min, 30 min and 60 min with (c, d, e) PP and (f, g, h) PMMA-An/TEMPO@PP separators, respectively.

materials are used as received.

2.2. Synthesis of PMMA-An and PMMA-An/TEMPO

Typically, 1.0 g of PMMA was dissolved in 9.0 mL of DMF, and 0.86 g of TEMPO and 0.31 g of AH were added successively. Then, the mixture was reacted for 12 h under magnetic stirring at 50 °C. After the reaction, it was slowly dropped into 20.0 mL of anhydrous ethanol, with the resulting sediment filtered and wished with anhydrous ethanol for three times. Then, the sediment was dried in a 70 °C vacuum oven for 12 h to obtain the PMMA precursor grafted with both AH and TEMPO groups, which was signed as pre-PMMA-AH/TEMPO. Subsequently, 4.0 g of pre-PMMA-AH/TEMPO, 2.78 g of An, 1.53 g of DMAP and 2.40 g of EDC.HCl were dissolved in 36.0 mL of DMF, and then placed in dark for reaction at room temperature under magnetic stirring for 24 h. The obtained precipitate was filtered and washed with anhydrous ethanol for three times and dried in a 70 °C vacuum oven for 12 h to obtain PMMA grafted with both An and TEMPO groups, signed as pre-PMMA-An/TEMPO. The PMMA-An precursor without TEMPO group was also obtained by the same preparation procedures.

2.3. Fabrication of porous PMMA-An/TEMPO@PP composite separators

Typically, 1.0 g of pre-PMMA-An/TEMPO was dissolved in 8.0 mL of DMF to prepare the precursor spinning solution. The PP separator was fixed on the collector in advance. During electrospinning, the key parameters were set as following: 0.08 mL h^{-1} of solution feeding rate, 15 kV of applied direct-current voltage, and 15 cm of distance between the needle and collector. The as-obtained pre-PMMA-An/TEMPO nanofiber coated PP membrane, signed as pre-PMMA-An/TEMPO@PP, was dried at 80 °C in a vacuum oven. Then, it was transferred to the UV curing box and exposed to UV light at an intensity of 0.02 W cm^{-2} for 2 h to obtain the cross-linked PMMA-An/TEMPO@PP membrane. The PMMA-An@PP membrane was also obtained for comparison.

2.4. Characterizations

The chemical structures and compositions of the samples were characterized by Fourier transform infrared (FTIR, NicoletIn10MX/Nicolet 6700, Thermo Fisher, USA), thermogravimetric analyzer (TGA, NETZSCH TG 209 F1 Libra®, Germany) with a temperature ramp of 10 °C min^{-1} under Ar atmosphere, respectively. Morphologies of all samples were observed using field-emission scanning electron microscope (FESEM, HitachiS-8010, Japan). X-ray photoelectron spectroscopy (XPS) was measured by Thermo Scientific ESCALAB 250Xi equipped with Al K_α X-ray source at an energy of 1486.6 eV. Electron spin resonance (ESR) spectrum was measured on a Bruker EMX plus. UV-cross-linking experiments were performed at room temperature (RT) using an Omnicure® S1500 Spot UV Light Curing System (Excelitas Technologies) equipped with a 200 W Hg arc lamp which irradiates with a wavelength range of 320–500 nm. In-situ optical observation was measured by LIB-MS cell (Beijing Science Star technology Co. Ltd.).

2.5. Electrochemical tests

All electrochemical measurements were carried out at room temperature using a CR2032 coin cell. The electrolyte used for Li deposition was 30 μL of 1.0 M lithium bis (trifuoromethanesulfonyl) imide (LiTFSI) in a mixture of 1,3-dioxalane and dimethyl ether (1:1 by volume) with 1 wt% $LiNO_3$ additive. The linear sweep voltammetry (LSV) measurement was performed by using Li foil as the counter electrode and a stainless-steel disc as the working electrode, while the separator was sandwiched

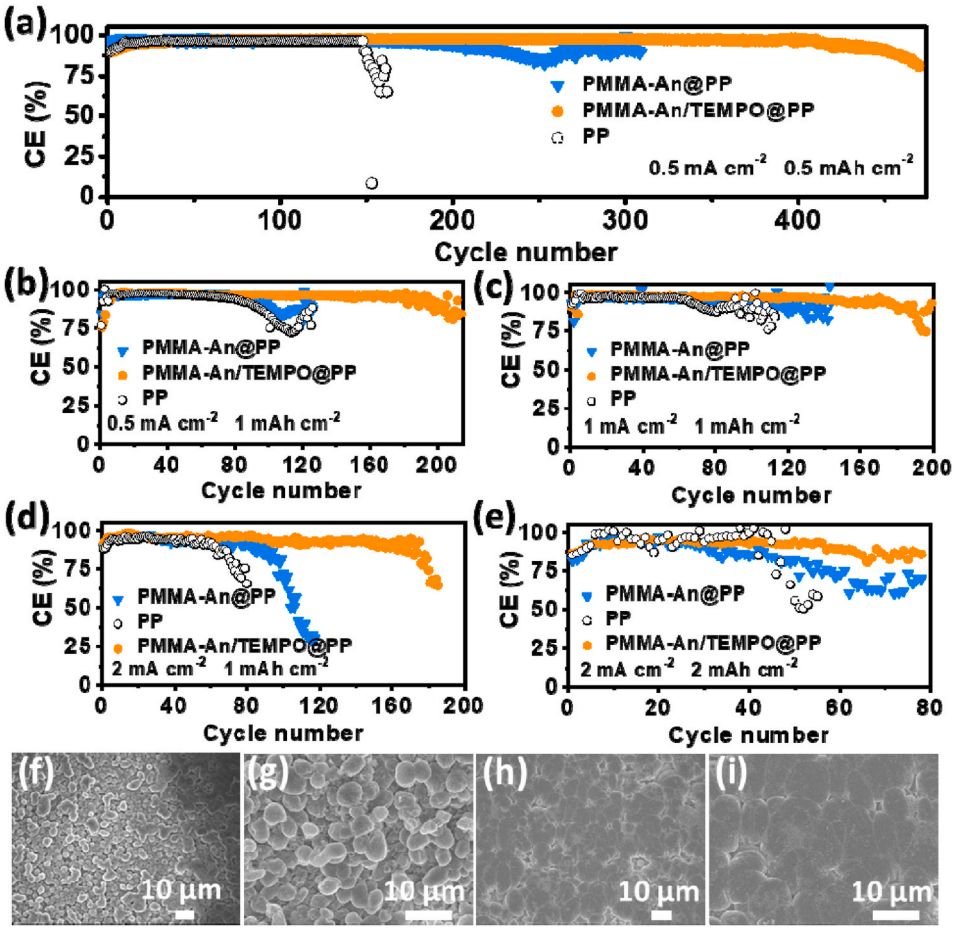

Fig. 3. Coulombic efficiencies of the Li|Cu cells with PP and PMMA-An/TEMPO@PP separators at different current densities and capacities: (a) 0.5 mA cm^{-2}, 0.5 mAh cm^{-2}; (b) 0.5 mA cm^{-2}, 1 mAh cm^{-2}; (c) 1 mA cm^{-2}, 1 mAh cm^{-2}; (d) 2 mA cm^{-2}, 1 mAh cm^{-2}; (e) 2 mA cm^{-2}, 2 mAh cm^{-2}. SEM images of Li metal anodes assembled with (f, g) PP and (h, i) PMMA-An/TEMPO@PP separators after 30 cycles at 1 mA cm^{-2} and 1 mAh cm^{-2}.

between the electrodes with the PMMA-An/TEMPO nanofiber side facing the Li foil. Coulomb efficiency was calculated as the ratio of stripping to plating capacity. With two layers of lithium foils as the working electrodes and PMMA-An/TEMPO@PP as the separator, the symmetrical Li|Li cell was also assembled. To prepare the $LiFePO_4$ electrode, $LiFePO_4$, carbon black, and PVDF at a weight ratio of 8:1:1 were mixed in NMP to form a uniform coating layer on the copper foil. Then, the full cell was assembled using $LiFePO_4$ electrode as cathode, lithium foil as anode, and PMMA-An/TEMPO@PP or PP as separator, respectively.

3. Results and discussion

Fig. 1a depicts the schematic preparation diagrams of pre-PMMA-An/TEMPO@PP and PMMA-An/TEMPO@PP separators. First, the pre-PMMA-An/TEMPO nanofibers with smooth surface morphology are uniformly deposited on the PP collector by electrospinning to obtain pre-PMMA-An/TEMPO@PP composite membrane. Then, PMMA-An/TEMPO@PP is obtained after the crosslinking of An in PMMA-An/TEMPO by ultraviolet light. Fig. 1b shows the optical photographs of PMMA-An/TEMPO@PP and PP separators. The surface morphologies of pre-PMMA-An/TEMPO@PP, PMMA-An/TEMPO@PP and PMMA-An@PP nanofiber membranes are examined by SEM. As shown in Fig. 1c, the pre-PMMA-An/TEMPO@PP nanofibers display a relatively uniform diameter of about 600 nm, which interconnect with each other into a three-dimensional porous network structure. Fig. 1d and e shows the top side of PMMA-An/TEMPO@PP composite separator after ultraviolet cross-linking treatment. Obviously, there are cross-linking points between the PMMA-An/TEMPO nanofibers in PMMA-An/TEMPO@PP. Compared to pre-PMMA-An/TEMPO nanofibers, the diameter of PMMA-An/TEMPO almost has no change while the pores become more uniform and smaller due to the denser nanofiber membranes after cross-linking reaction. For comparison, the same proportion of An has been grafted onto PMMA to obtain PMMA-An nanofiber coated PP separator, which is called PMMA-An@PP. Compared to PMMA-An/TEMPO@PP, PMMA-An@PP has similar fibrous morphology, microporous distribution and network structure (Fig. S1). The wettability of electrolyte has a significant effect on the distribution of lithium ions in the electrode and plays a crucial role in the growth of Li dendrites. As displayed in Fig. 1f, the PP separator shows poor electrolyte wettability, with a large contact angle of 40° after 30 s. In sharp contrast, the PMMA-An/TEMPO@PP separator shows good affinity toward electrolyte (1.0 M LiTFSI in DME: DOL = 1: 1 vol% with 5.0% $LiNO_3$) with immediate infiltration within 1 s, which indicates the greatly improved wettability of PMMA-An/TEMPO@PP separator toward electrolyte for the abundant polar functional groups.

To further determine the chemical composition and contents of functional groups including nitroxyl radical and carbonyl groups in different separators, FTIR spectra are obtained. As shown in Fig. S2a, the functional groups of An and TEMPO are indicated to be successfully grafted onto PMMA. The typical absorption peaks at 1730 cm^{-1} and 701 cm^{-1} are attributed to the C═O stretching and N–H wagging vibrations of amide groups in PMMA-An/TEMPO@PP and PMMA-An@PP separators respectively [36]. The strong absorption peak of PMMA-An/TEMPO@PP at 1365 cm^{-1} can be ascribed to the typical stretching vibration of nitroxyl radical [37,38]. Obviously, large number of polar functional groups, including C═O and nitroxyl radical groups,

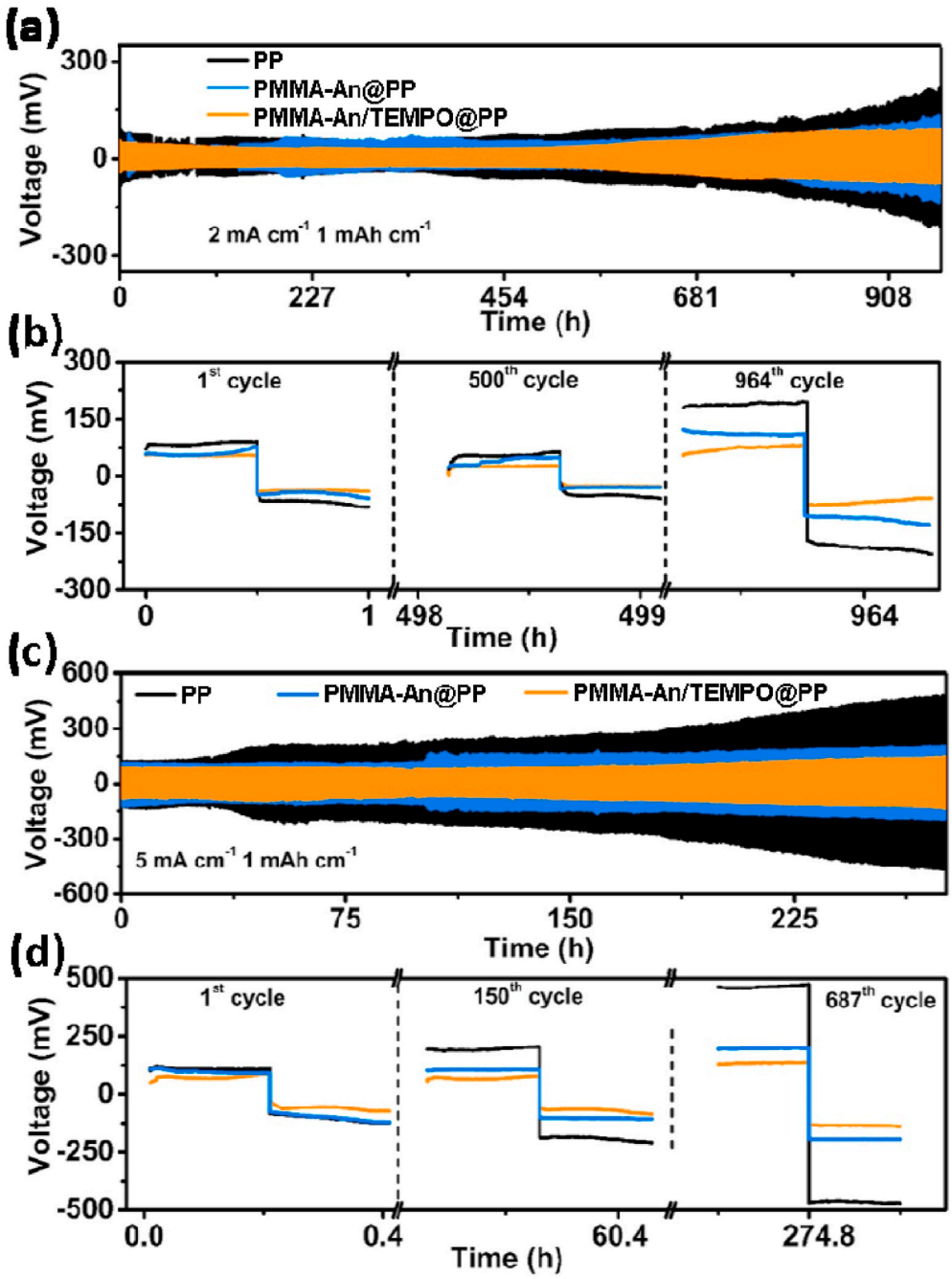

Fig. 4. Cycling voltage profiles of the symmetrical cells using PP and PMMA-An/TEMPO@PP separators under different current densities with a fixed capacity of 1 mAh cm^{-2}: (a) 2 mA cm^{-2}, (c) 5 mA cm^{-2}. (b, d) The corresponding voltage profiles with different cycle numbers.

have been successfully introduced in the PMMA-An/TEMPO@PP composite separator. Fig. S2b displays the ESR spectrum of PMMA-An/TEMPO@PP separator. The broad featureless ESR spectrum of PMMA-An/TEMPO@PP is caused by the large amount of unpaired electrons in polymers, which leads to a spin−spin interaction between the locally populated unpaired electrons [39]. The ESR spectrum provides credible evidence for the existence of radical species in PMMA-An/TEMPO@PP composite separator. In the XPS spectra, the high-resolution N 1s of PMMA-An/TEMPO@PP certifies the existence of TEMPO with typical peaks at 401.2 eV and 399.6 eV (Fig. S3a), which are assigned to the nitroxyl radical (nitroxyl radical) and C–N bond respectively [40]. The peak at 288.5 eV in the high-resolution C 1s spectrum are corresponding to the amide groups (Fig. S3b).

Due to the inevitable roughness of the electrode surface, the electric field distribution near the surface is not uniform. In the case of PP separator, the charge accumulates at the tip and directs Li^+ to preferentially deposit at the tip (Fig. 2a), which leads to the accelerated vertical growth instead of flat growth of deposited Li and eventually causes the formation of Li dendrites. In complete difference, the abundant polar functional groups in the PMMA-An/TEMPO@PP separator can evenly redistribute lithium ions when they pass through the functionalized separator, which will efficiently prevent the accumulation of Li^+ at the tip and achieve molecular-level homogeneous distribution (Fig. 2b). More importantly, the strong lithiophilic characteristic of nitroxyl radicals also endows the porous PMMA-An/TEMPO@PP composite separator with significant electric pumping feature, which can largely accelerate the lithium ion transport and thus reduce the resistance. Therefore, the symmetric Li|Li cell with PMMA-An/TEMPO@PP

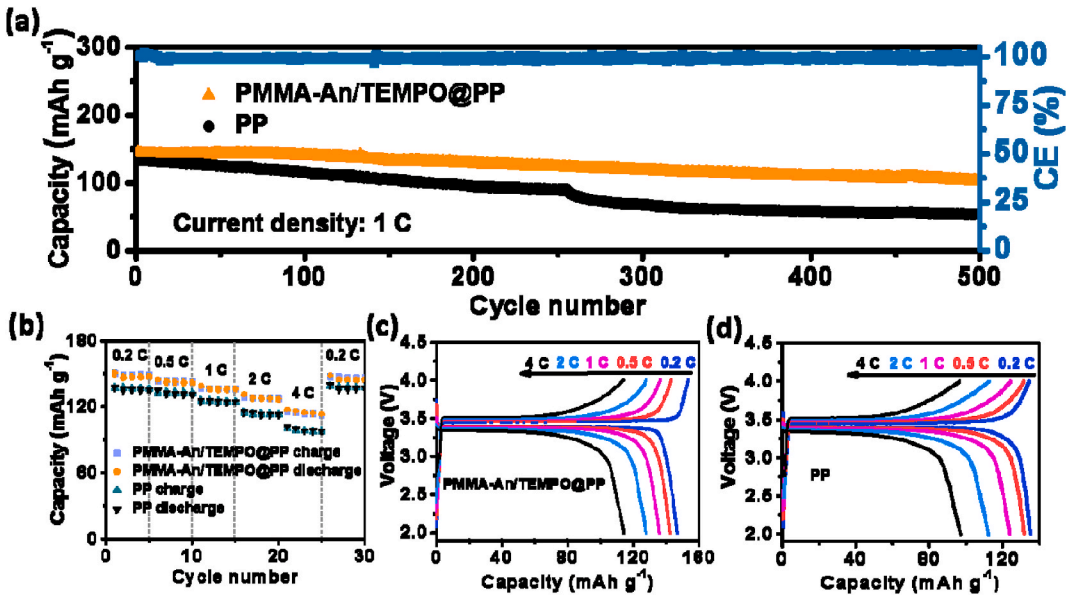

Fig. 5. Electrochemical performance of the Li/LFP cells with PP and PMMA-An/TEMPO@PP separators: (a) Cycling performance at 1.0 C. (b) Rate capability for cycling from 0.2 C to 4.0 C. The corresponding galvanostatic charge/discharge voltage profiles for rate testing with (c) PMMA-An/TEMPO@PP and (d) PP.

separator shows a lower interfacial impedance (21 Ω) than that (59 Ω) of PP separator (Fig. S4a), verifying the effect of PMMA-An/TEMPO@PP separator in enhancing Li^+ transport kinetics. Moreover, the linear sweep voltammetry (LSV) test shows that the PMMA-An/TEMPO@PP separator has a high electrochemical stability for Li^+/Li at 4.7 V (Fig. S4b), being much higher than that (3.8 V) of the PP separator.

In order to investigate the mechanism of PMMA-An/TEMPO@PP separator for leading Li electro-crystallization nucleation, Li is deposited at 1 mA cm^{-1} for 10 min, 30 min and 60 min respectively. As presented in Fig. 2c and f, Li nuclei are uniformly distributed after deposition for 10 min when PMMA-An/TEMPO@PP composite membrane separator is used as compared with PP separator. When the deposition time reaches 30 min, lithium dendrites have formed on the lithium metal anode with PP as separator, while the lithium nuclei are still evenly distributed on the lithium metal anode with PMMA-An/TEMPO@PP as separator (Fig. 2d and g). As the deposition continues, large number of lithium dendrites forms on the Cu foil when PP is used as separator, while the diameter of lithium nucleus keeps slow growth without lithium dendrites generated on the Cu foil by using PMMA-An/TEMPO@PP as separator (Fig. 2e and h). The obvious comparisons firmly demonstrate the polar groups contained in PMMA-An/TEMPO@PP composite separator can effectively guide the uniform nucleation of Li. The dynamic morphology evolution of deposited Li is also studied by in-situ optical observation at a current density of 5 mA cm^{-2} by using Li metal as anode, bare Cu foil as cathode, and PMMA-An/TEMPO@PP or PP as separators (Fig. S5). Obviously, a lot of dendritic Li appears in the PP cell, resulting in an uneven and porous lithium deposition layer. In contrast, more smooth and uniform Li deposition can be achieved on the Cu foil substrate with PMMA-An/TEMPO@PP separator even after 7 min of electrodeposition.

To evaluate the reversibility of lithium metal anode which is closely related to the formation of SEI and the growth of dendrite, the Coulombic efficiency is measured in Li|Cu cells. As shown in Fig. 3a, the Li|Cu cell with PMMA-An/TEMPO@PP separator shows a steady Coulombic efficiency of 97% with stable plating/stripping voltage profiles for more than 400 cycles at a current density of 0.5 mA cm^{-2}. Furthermore, the cell using PMMA-An/TEMPO@PP separator also exhibits higher Coulombic efficiency and cycle stability at all current densities, which are superior to those of the cells with PP and PMMA-An@PP separators (Fig. 3b–e and S6a). The stable Coulombic efficiency of PMMA-An/TEMPO@PP-based cell suggests that the irreversible consumption of lithium has been distinctly suppressed. In addition, the Li|Cu cell using PMMA-An/TEMPO@PP separator demonstrates a smaller voltage hysteresis than that with the PP separator (Fig. S6b). The morphologies of lithium deposition after 30 cycles at 1 mA cm^{-2} and 1 mAh cm^{-2} using PP (Fig. 3f and g) and PMMA-An/TEMPO@PP (Fig. 3h and i) separators further confirm that much denser lithium nucleus are formed when PMMA-An/TEMPO@PP is used as separator, indicating that the reversibility of lithium plating and striping is largely enhanced.

The cyclic performance of PMMA-An/TEMPO@PP and PP as separators is investigated by galvanostatic charge/discharge tests. As shown in Fig. 4a–d, symmetrical cells are tested at 2 or 5 mA cm^{-2} with a fixed capacity of 1 mA h cm^{-1}. The cell with PMMA-An/TEMPO@PP separator exhibits stable voltage profiles and small hysteresis, which are superior to those of the cells using PP and PMMA-An@PP separators. However, the cell with PP separator shows a gradual increase in hysteresis over cycles (Fig. 4b and d). The stable voltage distribution and small hysteresis of PMMA-An/TEMPO@PP-based cell are attributed to the reduced ion concentration gradient and stabilization of SEI formation. This superiority is especially evident at a high current density of 5 mA cm^{-2} (Fig. 4c). The cell with PP separator demonstrates higher hysteresis and undulatory cycling plateaus in both Li plating and striping processes. In obvious contrast, more stable and smooth voltage plateaus are obtained in the cell with PMMA-An/TEMPO@PP separator.

Finally, the performance of PMMA-An/TEMPO@PP separator is investigated in the full cell by coupling with LFP as cathode. Long-term cyclabilities of Li|LFP cells at 1.0 C with PMMA-An/TEMPO@PP or PP separators are shown in Fig. 5a. The initial discharge capacity of both cells is the same. However, the capacity of the cell with PP separator significantly decreases after 500 cycles, while the cell with PMMA-An/TEMPO@PP separator delivers a stable cyclability with 73% capacity retention at 1.0 C. The Li|LFP cell with PMMA-An/TEMPO@PP separator also shows enhanced rate performance than the cell with PP separator. As displayed in Fig. 5b–d, the Li|LFP cell with PMMA-An/TEMPO@PP separator renders the discharge capacities of 127 mA h g^{-1} at 2.0 C and 114 mA h g^{-1} at 4.0 C, respectively. All the above excellent performance of PMMA-An/TEMPO@PP separator in the Li|LFP cell proves its great potential as high-performance separators in high-energy LMBs.

4. Conclusions

In summary, a radical functionalized porous PMMA-An/TEMPO@PP composite membrane has been constructed by the direct electrospinning of PMMA-An/TEMPO nanofibers on the surface of PP separator. The lithiophilic functional groups of C═O and nitroxyl radical efficiently achieve the homogenization of lithium nucleation on the Cu foil, while the cross-linked An groups largely improve the mechanical strength of the nanofibrous PMMA-An/TEMPO coating layer. Therefore, the functional porous PMMA-An/TEMPO@PP composite separator not only exhibits excellent structural stability, but also guides the uniform and fast Li^+ flux at the molecular level. Consequently, it enables the uniform deposition of dendrite-free Li, as well as high Coulombic efficiency and ultralong-term reversible plating/stripping of Li in potential lithium metal battery applications.

CRediT authorship contribution statement

Chunyang Zhou: Conceptualization, Methodology, Investigation, Formal analysis, Data curation, Visualization, Writing – original draft, Writing – review & editing. **Wei Zong:** Investigation. **Gangyong Zhou:** Investigation. **Xiaoshan Fan:** Writing – review & editing. **Yue-E Miao:** Writing – review & editing, Supervision, Funding acquisition.

Declaration of competing interest

The authors declare that they have no known competing financial interests or personal relationships that could have appeared to influence the work reported in this paper.

Acknowledgements

The authors are grateful for the financial support from the National Natural Science Foundation of China (22075042), Natural Science Foundation of Shanghai (20ZR1401400, 18ZR1401600).

Appendix A. Supplementary data

Supplementary data to this article can be found online at https://doi.org/10.1016/j.coco.2021.100696.

References

[1] M.C. Stan, J. B, A. Kolesnikov, B. Wankmiller, J.E. Frerichs, M.R. Hansen, P. Bieker, M. Kolek, M. Winter, Sputter coating of lithium metal electrodes with lithiophilic metals for homogeneous and reversible lithium electrodeposition and electrodissolution, Mater. Today 39 (2020) 137–145.
[2] Z. Luo, C. Liu, Y. Tian, Y. Zhang, Y. Jiang, J. Hu, H.S. Hou, G.Q. Zou, X.B. Ji, Dendrite-free lithium metal anode with lithiophilic interphase from hierarchical frameworks by tuned nucleation, Energy Storage Mater 27 (2020) 124–132.
[3] R. Xu, X.Q. Zhang, X.B. Cheng, H.J. Peng, C.Z. Zhao, C. Yan, J.Q. Huang, Artificial soft–rigid protective layer for dendrite-free lithium metal anode, Adv. Funct. Mater. 28 (2018) 1705838.
[4] Y.F. Wang, L. Zhang, H.Q. Hou, W.H. Xu, G.G. Duan, S.J. He, K.M. Liu, S.H. Jiang, Recent progress in carbon-based materials for supercapacitor electrodes: a review, J. Mater. Sci. 56 (2021) 173–200.
[5] X.L. Yang, J.W. Wang, H.T. Guo, L. Liu, W.H. Xu, G.G. Duan, Structural design toward functional materials by electrospinning: a review, E-Polymers 20 (2020) 682–712.
[6] J.J. Yu, S.W. Liu, G.G. Duan, H. Fang, H.Q. Hou, Dense and thin coating of gel polymer electrolyte on sulfur cathode toward high performance Li-sulfur battery, Compos. Commun. 239 (2020) 239–245.
[7] H.Q. Yang, S.W. Liu, L.H. Cao, S.H. Jiang, H.Q. Hou, Superlithiation of non-conductive polyimide toward high-performance lithium-ion batteries, J. Mater. Chem.A 6 (2018) 21216–21224.
[8] S.W. Liu, H.Q. Yang, L. Sui, S.H. Jiang, H.Q. Hou, Self-adhesive polyimide (PI) @reduced graphene oxide (RGO)/PI@carbon nanotube (CNT) hierarchically porous electrodes: maximizing the utilization of electroactive materials for organic Li-ion batteries, Energy Technol. 8 (2020) 2000397.
[9] B. Liu, J.G. Zhang, W. Xu, Advancing lithium metal batteries, Joule 2 (2018) 833–845.
[10] G.Y. Zhou, L.L. Mo, C.Y. Zhou, Y. Lv, Y. E Miao, T.X. Liu, Flexible naphthalene-based polyimide nanofiber cathode with hierarchical micro/nanoporous structure for high-performance organic sodium-ion batteries, Compos. Commun. 22 (2020) 100490.
[11] S.Q. Wang, L. Xia, L. Yu, L. Zhang, H.H. Wang, X.W. Lou, Free-standing nitrogen-doped carbon nanofiber films: integrated electrodes for sodium-ion batteries with ultralong cycle life and superior rate capability, Adv. Energy Mater. 6 (2016) 1502217.
[12] L.L. Wang, F. Liu, W. L, S. Shao, Z. Cui, Y.M. Zhao, Y.M. Zhou, J.X. He, Graphite oxide dopping polyimide nanofiber membrane via electrospinning for high performance lithium-ion batteries, Compos. Commun. 16 (2019) 150–157.
[13] L. Wei, L. Li, T. Zhao, N.X. Zhang, Y.Y. Zhao, F. Wu, R.J. Chen, MOF-derived lithiophilic CuO nanorod arrays for stable lithium metal anodes, Nanoscale 12 (2020) 9416–9422.
[14] P.J. Kim, V.G. Pol, High performance lithium metal batteries enabled by surface tailoring of polypropylene separator with a polydopamine/graphene layer, Adv. Energy Mater. 8 (2018) 1802665.
[15] A. Hussain, D. Li, Y. Luo, H.Z. Zhang, H. Zhang, X. Li, Porous membrane with improved dendrite resistance for high-performance lithium metal-based battery, J. Membr. Sci. 605 (2020) 118108.
[16] R.J. Pan, X.X. Xu, R. Sun, Z.H. Wang, J. Lindh, K. Edström, M. Strømme, L. Nyholm, Nanocellulose modified polyethylene separators for lithium metal batteries, Small 14 (2018) 1704371.
[17] J. Zhi, S.K. Li, M. Han, P. Chen, Biomolecule-guided cation regulation for dendrite-free metal anodes, Sci. Adv. 6 (2020), eabb1342.
[18] J. Oh, H. Jo, H. Lee, H. Kim, Y.M. Lee, M. Ryou, Polydopamine-treated three-dimensional carbon fiber-coated separator for achieving high-performance lithium metal batteries, J. Power Sources 430 (2019) 130–136.
[19] H.D. Shi, J.Q. Qin, K. Huang, P.F. Lu, Z.S. Wu, Two-dimensional mesoporous polypyrrole-graphene oxide heterostructure as dual-functional ion redistributor for dendrite-free lithium metal anodes, Angew. Chem. Int. Ed. 59 (2020) 12147–12153.
[20] D.C. Lin, Y.Y. Liu, A. Pei, Y. Cui, Nanoscale perspective: materials designs and understandings in lithium metal anodes, Nano Res 10 (2017) 4003–4026.
[21] A. Wang, X. Zhang, Y.W. Yang, J. Huang, X. Liu, J. Luo, Horizontal centripetal plating in the patterned voids of Li/graphene composites for stable lithium-metal anodes, Inside Chem. 4 (2018) 2192–2200.
[22] C.Y. Cui, C.Y. Yang, N. Eidson, J. Chen, F.D. Han, L. Chen, C. Luo, P.F. Wang, X. L. Fan, C.S. Wang, A highly reversible, dendrite-free lithium metal anode enabled by a lithium-fluoride-enriched interphase, Adv. Mater. 32 (2020) 1906427.
[23] X.F. Wang, G. Pawar, Y.J. Li, X.D. Ren, M.H. Zhang, B.Y. Lu, A. Banerjee, P. Liu, E. J. Dufek, J.G. Zhang, J. Xiao, J. Liu, B. Liaw, Glassy Li metal anode for high-performance rechargeable Li batteries, Nat. Mater. 19 (2020) 1339–1345.
[24] C.F. Ding, X.W. Fu, H. Li, J.Y. Yang, J.L. Lan, Y.H. Yu, W.H. Zhong, X.P. Yang, An ultrarobust composite gel electrolyte stabilizing ion deposition for long-life lithium metal batteries, Adv. Funct. Mater. 29 (2019) 1904547.
[25] H.J. Zhao, N.P. Deng, W.M. Kang, Z.J. Li, G. Wang, B. Cheng, Highly multiscale structural Poly(vinylidene fluoridehexafluoropropylene)/polym-phenyleneisophthalamide separator with enhanced interface compatibility and uniform lithium-ion flux distribution for dendrite-proof lithium-metal batteries, Energy Etorage Mater 26 (2020) 334–348.
[26] C.F. Li, S.H. Liu, C.G. Shi, G.H. Liang, Z.T. Lu, R.W. Fu, D.C. Wu, Two-dimensional molecular brush-functionalized porous bilayer composite separators toward ultrastable high-current density lithium metal anodes, Nat. Commun. 10 (2019) 1363.
[27] C.Z. Zhao, P.Y. Chen, R. Zhang, X. Chen, B. Li, X.Q. Zhang, X. Cheng, Q. Zhang, An ion redistributor for dendrite-free lithium metal anodes, Sci. Adv. 4 (2018) eaat3446.
[28] H.D. Yuan, J. Nai, H. Tian, Z. Ju, W. Zhang, Y. Liu, X. Tao, X.W. Lou, An ultrastable lithium metal anode enabled by designed metal fluoride spansules, Sci. Adv. 6 (2020) eazz3112.
[29] X.Z. Huang, R. He, M. Li, M.O.L. Chee, P. Dong, J. Lu, Functionalized separator for next-generation batteries, Mater. Today 41 (2020) 143–155.
[30] Y.D. Pan, S.L. Chou, H.K. Liu, S.X. Dou, Functional membrane separators for next-generation high-energy rechargeable batteries, Natl. Sci. Rev. 4 (2017) 917–933.
[31] K.E.K. Sun, T.K.A. Hoang, T.N.L. Doan, Y. Yu, X. Zhu, Y. Tian, P. Chen, Suppression of dendrite formation and corrosion on zinc anode of secondary aqueous batteries, ACS Appl. Mater. Interfaces 9 (2017) 9681–9687.
[32] D.C. Lin, Y.Y. Liu, Y. Cui, Reviving the lithium metal anode for high-energy batteries, Nat. Nanotechnol. 12 (2017) 194–206.
[33] L.D. Shen, X. Liu, J. Dong, Y.T. Zhang, C.X. Xu, C. Lai, S.Q. Zhang, Functional lithiophilic polymer modified separator for dendrite-free and pulverization-free lithium metal batteries, J. Energy Chem. 52 (2021) 262–268.
[34] X.B. Cheng, R. Zhang, C.Z. Zhao, Q. Zhang, Toward safe lithium metal anode in rechargeable batteries: a review, Chem. Rev. 117 (2017) 10403–10473.
[35] C.Y. Yan, P. Zhu, H. Jia, J.D. Zhu, R.K. Selvan, Y. Li, X. Dong, Z. Du, I. Angunawela, N.Q. Wu, M. Dirican, X.W. Zhang, High-performance 3D fiber network composite electrolyte enabled with li-ion conducting nanofibers and amorphous PEO-based cross-linked polymer for ambient all-solid-state lithium-metal batteries, Adv. Fiber Mater. 1 (2019) 46–60.
[36] Y.H. Ding, P. Zhang, Z.L. Long, Y. Jiang, F. Xu, W. Di, The ionic conductivity and mechanical property of electrospun P(VDF-HFP)/PMMA membranes for lithium ion batteries, J. Membr. Sci. 329 (2009) 56–59.
[37] W. Guo, J. Su, Y.H. Li, L.J. Wan, Y.G. Guo, Nitroxide radical polymer/graphene nanocomposite as an improved cathode material for rechargeable lithium batteries, Electrochim. Acta 72 (2012) 81–86.
[38] H.F. Li, Z.X. Liu, G.J. Liang, Y. Huang, Y. Huang, M.S. Zhu, Z.X. Pei, Q. Xue, Z. J. Tang, Y.K. Wang, B.H. Li, C.Y. Zhi, Waterproof and tailorable elastic

rechargeable yarn zinc ion batteries by a cross-linked polyacrylamide electrolyte, ACS Nano 12 (2018) 3140–3148.

[39] Y.J. Li, Z.K. Jian, M.D. Lang, C.M. Zhang, X.Y. Huang, Covalently functionalized graphene by radical polymers for graphene-based high-performance cathode materials, ACS Appl. Mater. Interfaces 8 (2016) 17352–17359.

[40] F. Geneste, C. Moinet, S.A. Girardb, F. Solalb, Covalent attachment of TEMPO onto a graphite felt electrode and application in electrocatalysis, New J. Chem. 29 (2005) 1520–1526.